AGU ADVANCING EARTH AND SPACE SCIENCES

Water Resources Research®

RESEARCH ARTICLE

Key Points:

- This study investigates the combined effects of wellbore storage and non-Darcy flow in pumping well systems using a multiphysics model
- The findings reveal the expansion of nonlinear flow regions, transition to a quasi-steady-state, and the gradual shift toward Darcy flow
- The study highlights the formation of vortices and 2D flow near the wellbore, which affect flow paths and hydraulic pressure consumption

Author Contributions:

Conceptualization: Yu He, Haiying Huang, Deyi Hou, Jian Luo
Formal analysis: Yu He, Quan Guo, Yuzheng Liu
Funding acquisition: Jian Luo
Investigation: Yu He
Methodology: Yu He, Deyi Hou, Jian Luo
Project Administration: Jian Luo
Software: Yu He
Supervision: Jian Luo
Validation: Quan Guo, Yuzheng Liu, Haiying Huang
Writing – original draft: Yu He

Multiphysics Modeling Investigation of Wellbore Storage Effect and Non-Darcy Flow

Yu He[1] , Quan Guo[1] , Yuzheng Liu[1], Haiying Huang[1], Deyi Hou[2] , and Jian Luo[1]

[1]School of Civil and Environmental Engineering, Georgia Institute of Technology, Atlanta, GA, USA, [2]School of Environment, Tsinghua University, Beijing, China

Abstract This study presents a comprehensive investigation of wellbore storage effects and non-Darcy flow in pumping well systems using a multiphysics numerical model. The model incorporates the Reynolds-averaged Navier-Stokes equations coupled with a moving free surface to simulate the flow field and drawdown in the wellbore. Hydraulic behavior of the system, including well and aquifer drawdown, pumped water ratio, aquifer flow nonlinearity, and wellbore flow field, is analyzed and compared with simplified 1-D models. This study highlights the presence of a vortex in the wellbore flow field induced by large Reynolds number and the uneven stress distribution at the screen. This vortex influences the wellbore drawdown and introduces 2-D flow in the surrounding aquifer, which further contributes to the longer travel paths for groundwater particles and increased hydraulic pressure consumption. The results show that non-Darcy flow, coupled with wellbore storage effects, leads to higher drawdown in the pumping well compared to Darcy flow cases. The aquifer drawdown exhibits a similar temporal pattern but with decreasing deviation at larger distances due to the cone of depression. The pumped water ratio indicates the challenge of supplying outflow at the intake from aquifer storage, with nonlinear flow resulting in a smaller ratio compared to linear cases. A nonlinearity ratio is defined to illustrate the expansion of nonlinear flow regions over time, their convergence to a predictable quasi-steady-state shape, which is influenced by the Forchheimer parameter, and the gradual transition to Darcy flow away from the wellbore.

Plain Language Summary This study focuses on understanding the behavior of water flow in pumping wells considering two important factors: wellbore storage and non-Darcy flow. Wellbore storage refers to the amount of water stored inside the well, while non-Darcy flow describes the flow behavior in the surrounding aquifer. Using a computer model, the researchers found that as pumping continues, the areas of nonlinear flow expand and eventually settle into a stable pattern. This transition from nonlinear flow to a more predictable behavior is influenced by the properties of the aquifer. The study also revealed that the presence of wellbore storage and the flow patterns near the well have a significant impact on the overall hydraulic performance. These findings have practical implications for improving the design and operation of pumping wells.

1. Introduction

Well pumping is widely used in various geological engineering applications, such as groundwater extraction, subsurface remediation, and energy resource exploitation. Research on well hydraulics has a long history, with classic approaches and solutions that have provided benchmark results in hydrogeology. Notable examples include Hantush (1959), Moench and Prickett (1972), Neuman (1972), Papadopulos and Cooper (1967), and Theis (1935). These approaches and solutions are based on the assumption of linear or Darcy flow, where the hydraulic gradient and water flux exhibit a linear relationship with hydraulic conductivity. However, it is known that the Darcy flow assumption may not be valid at high Reynolds numbers (Re ≥ 10) in porous media (Bear, 1988). Forchheimer (1901) introduced the Forchheimer equation that incorporates a quadratic term in addition to the traditional flow equation to account for nonlinearity. Subsequent studies further investigated and validated the importance of considering non-Darcy flow in porous media (Z. X. Chen et al., 2001; Irmay, 1958; Thiruvengadam & Kumar, 1997; Whitaker, 1996).

Nonlinear flows with high velocities are commonly observed in well pumping systems, where the flow regime near the wellbore exhibits significant nonlinearity due to the increasing specific flow rate as it approaches the wellbore (Huang & Ayoub, 2008; Wu, 2002). While predicting steady-state drawdown behavior for such nonlinear flow

**Writing – review & editing:** Haiying Huang, Jian Luo

is relatively simple (Bear, 2012; Ewing et al., 1999), analyzing transient non-Darcy flow to a well presents challenges due to the complexity of the nonlinear flow equation (Mathias et al., 2008; Takhanov, 2011). To address this, several approximate solutions have been developed for non-Darcy flow. Moutsopoulos and Tsihrintzis (2005) derived an approximate similarity solution for one-dimensional large flow rates. Wen et al. (2008) employed a power law function and a time-dependent approximation term to describe non-Darcy flow, which converges with classic analytical solutions at large distances but may not be valid near the wellbore. Mathias et al. (2008) derived a solution using an asymptotic expansion technique that performs well at large times and away from the wellbore. They also developed a finite-difference solution for the transient state; however, the boundary condition at the screen lacked a proper physical interpretation and later proved to require an additional constraint for implementation in Text S1 in Supporting Information S1. The above solutions have limitations, especially in capturing the drawdown behavior at early times and near the wellbore, which remains relatively unexplored.

Wellbore storage is another important factor that adds complexity to well hydraulics in pumping test theory and analysis. The significance of well storage effects was recognized in large-diameter wells, where it was observed that these effects are prominent during the early stages of pumping (Papadopulos & Cooper, 1967). During the initial stage, most of the pumped water is supplied by the downward vertical casing flow, and its contribution gradually decreases to zero as pumping continues. The interplay between well geometry and aquifer characteristics governs this process (He et al., 2022; Hou & Luo, 2019; Martin-Hayden et al., 2014), leading to alterations in the hydraulic performance of the well. While the impact of wellbore storage on well hydraulics has been recognized, the flow field within the wellbore has often been neglected. Unlike well storage, which accounts for the pumped water from well casing and screen storage, the wellbore flow field refers to the velocity field generated by the pump intake suction and its influence on the aquifer flow field. It is reasonable to hypothesize that the flow field within the wellbore may significantly affect the aquifer flow near the wellbore and the drawdown behavior in the pumping well. In fact, VonHofe and Helweg (1998) conducted a field study on the flow velocity outside the well screen and concluded that the pump intake position has a non-negligible impact on the hydraulic performance of a production well, indicating that the flux is not evenly distributed along the screen. It has been demonstrated by C. Chen et al. (2003) that the conventional 1-D model assumption of imposing the screened well face as a uniform-flux boundary or a uniform-head boundary misrepresents the actual flux or pressure distribution along the horizontal wellbore. Wang and Zhan (2017a, 2017b) proposed a more realistic mixed-type boundary condition at the screen to study in-well head loss. However, the employed hybrid analytical-numerical method is limited to simulating 1-D wellbore flow. Unfortunately, the combined effect of the wellbore flow and wellbore storage has not been comprehensively considered in pumping test theory and analysis.

In this study, we aim to investigate the combined impact of non-Darcy flow and wellbore storage on the aquifer flow near the wellbore and the drawdown behavior in both the pumping well and the aquifer. Specifically, we will examine how the nonlinearity of the flow and the characteristics of wellbore storage influence the hydraulic performance of well systems in high Reynolds scenarios. The novelty of our study lies in the integration of the flow field within the wellbore described by the Reynolds-averaged Navier-Stokes (RANS) equations with the groundwater flow in the aquifer, using a multiphysics numerical model. To the best of our knowledge, this is the first time such a multiphysics model is being utilized to explore the effects of wellbore flow and non-Darcy flow. Additionally, we will investigate the potential for simplifying this complex multiphysics model while maintaining its accuracy and relevance. By conducting these numerical investigations, we aim to enhance our understanding of wellbore storage effects and non-Darcy flow, which will contribute to the advancement of well hydraulics and provide valuable insights for practical applications in various geological engineering activities.

2. Conceptual Model

Figure 1 depicts the conceptual model used in this study. We consider a common pumping scenario involving a fully-penetrating short screened well with a screen radius of r_w. The well operates at a constant pumping rate in a homogenous and isotropic confined aquifer that extends infinitely in the horizontal plane (Papadopulos & Cooper, 1967). The conceptual model can be extended to work with heterogenous and anisotropic formation by assigning a conductivity matrix in numerical simulations. The upper and lower boundaries of the aquifer domain are impermeable, preventing any flow across these boundaries. The pumping tube is positioned at the center of the well screen, which induces radial formation flow toward the wellbore. The impact of pump intake vertical position on sample origin and well hydraulic performance is a topic of considerable discussion (McMillan
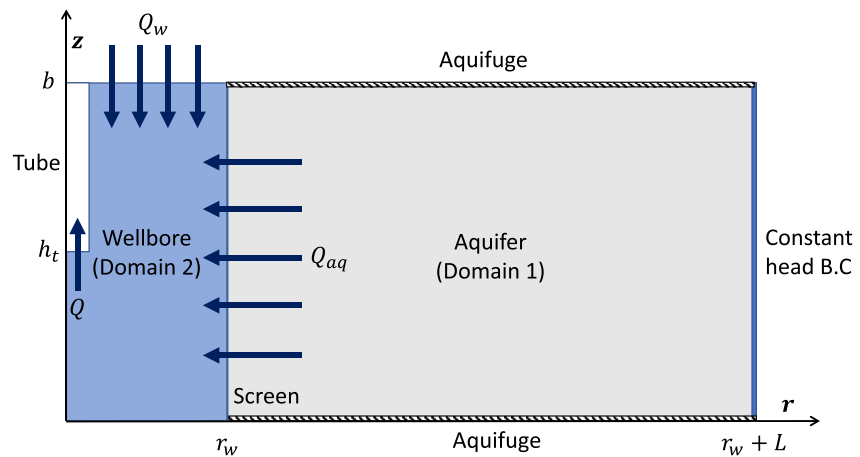
Figure 1. Schematic diagram of the axisymmetric conceptual model. Domain 1 and 2 simulate non-Darcy flow and wellbore flow, respectively.

et al., 2014; Nielsen, 2005; VonHofe & Helweg, 1998). Consequently, the movement of the pumping tube along the centering line within the well screen leads to changes in the wellbore mixing and flow field, which underscores the limitations inherent in the conventional 1-D model. To simplify the analysis, we adopt a 2-D axisymmetric flow model represented by the coordinates (r, φ, z). It is important to note that this study does not consider well loss and skin effect. This means that no pressure loss is accounted for due to formation flow through the screen, and there are no variations in permeability of the formation near the wellbore.

During pumping, the pumped water, Q, is comprised of two water sources: water from the wellbore storage, Q_w, and water from the formation, Q_{aq}. Thus, we investigate a multiphysics problem involving the interaction between wellbore flow and porous media flow during pumping. Two distinct domains are considered: Domain 2 represents the flow within the wellbore, while Domain 1 represents the flow in the porous media surrounding the wellbore. In Domain 2, we assume turbulent flow conditions due to the small length scale and high pumping rates, the values of which are similar to those described in the field study by VonHofe and Helweg (1998). To accurately account for the hydraulic losses and eddy behavior associated with turbulence dissipation, we employ the k-ϵ turbulence model. This model incorporates the concepts of turbulent kinetic energy and dissipation rate into the RANS equations, providing a comprehensive description of the turbulent flow dynamics within the wellbore. In Domain 1, we assume non-Darcy flow. Non-Darcy flow is a significant phenomenon in scenarios characterized by high Reynolds numbers near the wellbore, where the inertial and drag forces result in nonlinear flow behavior. It is worth noting that Martin-Hayden et al. (2014) employed a similar conceptual model to investigate groundwater sampling; however, their study focused on laminar flow and Darcy flow, neglecting the vertical flow from the well casing. In our study, we extend this conceptual model by incorporating turbulent flow conditions and considering the vertical flow from the well casing, enabling a more comprehensive understanding of the hydraulic behavior within the well system.

3. Numerical Modeling

3.1. Multiphysics Flow Model

Based on the conceptual model, the developed numerical model consists of an aquifer domain and a wellbore domain. The continuity equation in the aquifer domain is given by:

$$-\frac{S_s}{\rho g}\frac{\partial p_1}{\partial t} = \nabla \cdot \mathbf{q_1} \tag{1}$$

where t [T] is the pumping time, p_1 [$M/(LT^2)$] and $\mathbf{q_1}$ [L/T] are hydraulic pressure and flux vector in the aquifer domain, S_s [L^{-1}] is specific storativity, ρ [M/L^3] is water density, and g [L/T^2] is gravity constant.

The nonlinear relationship between the specific discharge and the pressure gradient is described by the Forchheimer's equation:

$$-\frac{K}{\rho g}\nabla p_1 = \mathbf{q_1} + \beta|\mathbf{q_1}|\mathbf{q_1} \tag{2}$$

Table 1
Hydrogeologic Parameters for the Base Case Model

Notation	Parameter	Value
Aquifer thickness	b	2 m
Aquifer lateral length	L	1,000 m
Pumping rate	Q	0.14 m³/s
Well radius (screen/casing)	$r_w = r_c$	0.3 m
Pumping tube radius	r_t	0.02 m
Aquifer conductivity	K	0.01 m/s
Aquifer specific storativity	S_s	1×10^{-3} 1/m
Forchheimer coefficient	C_F	0.55
Intake height	h_t	1 m
Initial hydraulic head	h_0	20 m
Wellbore Reynolds number	R_e	300,000

where K [L/T] is hydraulic conductivity. It is important to note that in low Reynolds number situations, the nonlinear terms become negligible and Darcy flow assumptions are sufficient.

The Forchheimer parameter β was investigated by various experimental and field studies (Muskat, 1937; Scheidegger, 1960). The solution proposed by Joseph et al. (1982) and Ward (1964) is used here:

$$\beta = C_F \sqrt{\frac{K\rho}{\mu g}} \tag{3}$$

where μ [$M/(LT)$] is dynamic viscosity of water, and C_F is a dimensionless coefficient. C_F ranges from 0 to 1 and is considered an indicator of groundwater flow nonlinearity. A typical value of C_F is 0.55 (Nield & Bejan, 2006).

In the wellbore domain, considering incompressible and Newtonian fluid, the flow field is described by the Reynolds-averaged Navier-Stokes equations (RANS). The k-ϵ turbulence model is used to simulate mean flow characteristics for turbulent flow conditions, RANS are modified to:

$$\rho \frac{\partial \boldsymbol{q_2}}{\partial t} + \rho(\boldsymbol{q_2} \cdot \nabla)\boldsymbol{q_2} = -\nabla p_2 + \nabla \cdot (\mu + \mu_t)\left(\nabla \boldsymbol{q_2} + (\nabla \boldsymbol{q_2})^T\right) + \rho g \tag{4}$$

where p_2 [$M/(L^1 T^2)$] and $\boldsymbol{q_2}$ [L/T] are pressure head and velocity vector in the wellbore domain, μ_t [$M/(LT)$] is the turbulent (eddy) viscosity at high Reynolds number.

$$\mu_T = \rho C_\mu \frac{k^2}{\epsilon} \tag{5}$$

where C_μ is a model constant. The model introduces two dependent variables: the turbulent kinetic energy, k [L^2/T^2], and the turbulent dissipation rate, ϵ [L^2/T^3]. Transport equations for the two variables can be found in Launder and Spalding (1974).

Casing walls and tube walls in the wellbore domain are considered smooth, that is, the friction factor is small. In fact, when the base case parameters from Table 1 are applied to the Darcy-Weisbach equation, the resulting head loss (<1 cm) is negligible. A lift-off is applied to casing and tube walls (no slip boundary condition) to accommodate turbulent flow, that is, a dimensionless distance of 11 between the computational domain and the physical wall is created. The law of the wall is verified using the cross-sectional velocity profile at the top of the screen, ensuring the validity of the turbulent simulation. Detailed explanation and figures can be found in Supporting Information S1 (Text S4 and Figure S6 in Supporting Information S1).

The wellbore domain and aquifer domain are coupled by setting equal flux and hydraulic pressure on both sides of the wellbore screen (r_w [L]), that is, pressure and flux continuity:

$$p_2(r_w, z, t) = p_1(r_w, z, t), \qquad \boldsymbol{q_2}(r_w, z, t) \cdot \boldsymbol{n_r} = \boldsymbol{q_1}(r_w, z, t) \cdot \boldsymbol{n_r} \tag{6}$$

where $\boldsymbol{n_r}$ is the unit vector in r-axis.

The outlet boundary is applied at the pumping tube intake, where a normal outflow velocity is imposed. The free surface movement in the wellbore can be described by the moving mesh:

$$\boldsymbol{u}_{\text{mesh}} \cdot \boldsymbol{n} = \boldsymbol{q_2} \cdot \boldsymbol{n}, \qquad p_{\text{at}} = p_2 \tag{7}$$

where $\boldsymbol{u}_{\text{mesh}}$ [L/T] indicates water column mesh velocity, p_{at} [$M/(L^1 T^2)$] is the atmosphere pressure, and $\boldsymbol{n}$ is the normal vector of the free surface motion. To control the attachment angle between the free surface and adjacent walls, surface tension force is included in momentum equation, with a specified contact angle of $\pi/2$ radians. The mesh resolution in the wall region is verified by maintaining a stable contact angel during the simulations.

3.2. Numerical Implementation

The numerical model is solved in a 2-D axisymmetric domain using COMSOL Multiphysics®, a finite element analysis and solver software, which has been extensively used as a reliable tool for simulating groundwater flow (Li et al., 2009; Singha & Loheide, 2011; Zanchini et al., 2012).

The wellbore fluid domain deformations are implemented to account for the motion of the air/fluid interface and the decline of hydraulic head. The moving mesh module is applied, constraining mesh displacement only by the domain boundaries. Here, no slip boundary condition is specified for casing walls and tube walls in the wellbore domain. The shape of the domain is governed by the explicit boundary conditions (the pumping tube, the free surface, and walls). Within the interior of the domain, the mesh is governed by a smoothing method. The Yeoh smoothing method (Rivlin & Rideal, 1948; Selvadurai, 2006; Yeoh, 1993) is employed to solve the deforming mesh. The method seeks to minimize mesh deformation energy. The strain energy density function is used to minimize deformation energy:

$$W = \frac{1}{2} \int_{\Omega} \sum_{i=1}^{3} C_i (I_1 - 3)^i + \kappa'(J - 1)^2 dV \tag{8}$$

where I_1 is the strain invariant of the Cauchy-Green deformation tensors, J is the determinant of the defamation gradient tensor, and κ' is the material bulk modulus. C_i are material constants, C_1 and C_3 are 1 and 0 for incompressible materials while stiffening factor C_2 of 10 controls the nonlinear stiffening of the material under deformation. Yeoh smoothing produces the best results and allows the largest displacement before elements become inverted. However, it can cause convergence problems due to its strong nonlinearity, particularly for the time-dependent solver. Thus, mesh configurations are optimized to address numerical stability.

Table 1 lists the typical hydrogeologic parameters for the base case model, which are based on typical values reported in Gutentag et al. (1984), the turbulent flow regime in the wellbore and the non-Darcy flow regime in the aquifer are confirmed by the Reynolds number. These parameters are utilized in all simulations conducted in this study unless otherwise stated. Preliminary sensitivity analysis was performed by varying the aquifer lateral length, ensuring that the constant head boundary is placed far enough to eliminate any boundary effect.

The model grid size decreases gradually from the aquifer constant head boundary toward the center of the borehole, with a maximum element size restriction of 0.01 m at the well screen. The wellbore domain, with a mesh area of 6 m², is separated into 5,454 irregular triangular elements, while the aquifer domain has 7,211 elements distributed across an area of 2,000 m². A mesh refinement study was performed to determine that the average element quality is adequate.

3.3. Dimensionless System

Typical dimensionless transformation of drawdown S [L] solutions are (Papadopulos & Cooper, 1967; Theis, 1935):

$$S_D = \frac{S}{Q/(4\pi T)} \tag{9}$$

$$t_D = \frac{t}{r_w^2 S_s b/(4T)} \tag{10}$$

$$r_D = \frac{r}{r_w} \tag{11}$$

It shall be noticed that in cylindrical coordinates, a pumping well yields negative radial flux, as shown in Figure 1. To establish a positive dimensionless system, Forchheimer parameter and the flux vector are defined as follows:

$$\beta_D = \frac{\beta}{2\pi b r_w/Q} \tag{12}$$

$$\boldsymbol{q}_D = (q_{rD}, 0, q_{zD}) = \frac{-q}{Q/(4\pi b r_w)} \tag{13}$$

where q represents both flux vectors q_1 and q_2 in aquifer and wellbore.

4. Hydraulic Behavior Analysis

4.1. Wellbore Flow Field

Figure 2 provides a visual representation of the simulated flow field in the wellbore and the two components of pumped water. The color-coded streamlines depict the flow direction and source, with green representing downward flow from the casing (wellbore storage) and blue representing formation inflow (aquifer storage). The moving-mesh method describes the decrease of the free surface in the wellbore. Cases with various aquifer storativity α (defined as $\alpha = S_s b$) are illustrated. The 2-D model demonstrates a more comprehensive and realistic representation of in-well hydraulics when compared to conventional 1-D analytical models. Integrated effects from wellbore storage and turbulent flow are clearly observed.

During the early pumping stage, well storage is a more tangible source compared to aquifer storage. In particular, the model with the lowest storativity has little formation water entering the screen. In contrast, for the highest α case, most of pumped water is from the formation inflow, indicating that aquifer flow has dominated the pumped water at this moment due to faster aquifer storage response. As pumping continues, the rate of wellbore drawdown increase slows down, leading to less downward flow from the well casing and more influent from the formation. This behavior is characterized by the dimensionless variable water flow ratio η_q, which will be further elaborated in Section 4.3. The large Reynolds number resulting from the parameters listed in Table 1 causes turbulence and the formation of a vortex (see the vorticity field in Figure S7 in Supporting Information S1) at the center of the screen at the intake position. Curved vortex lines, tangent to the local vorticity vector (in the θ direction in the 2-D asymmetric model), form a loop around the pumping tube. Through the time differentiation of the fluid circulation, Kevin's theorem is proved. The proof indicates that vortex occurs when the fluid is viscid and the integrated viscous force is non-zero around the contour of the local region. In practice, the conditions for vorticity creation via viscous torques often occur at solid boundaries where the no-slip condition is applied (Kundu et al., 2015). During the early pumping stage, the streamlines forming the vortex are mostly from the downward casing flow, especially for the low storativity case. However, as pumping progresses and the aquifer responds, the streamlines forming the vortex are dominated by the aquifer flow. The vortex and the pumping stress also accelerate the inflow velocity below the intake and decelerate the inflow velocity above the intake, leading a nonuniform entrance velocity profile, a detailed discussion is given in Section 4.5.

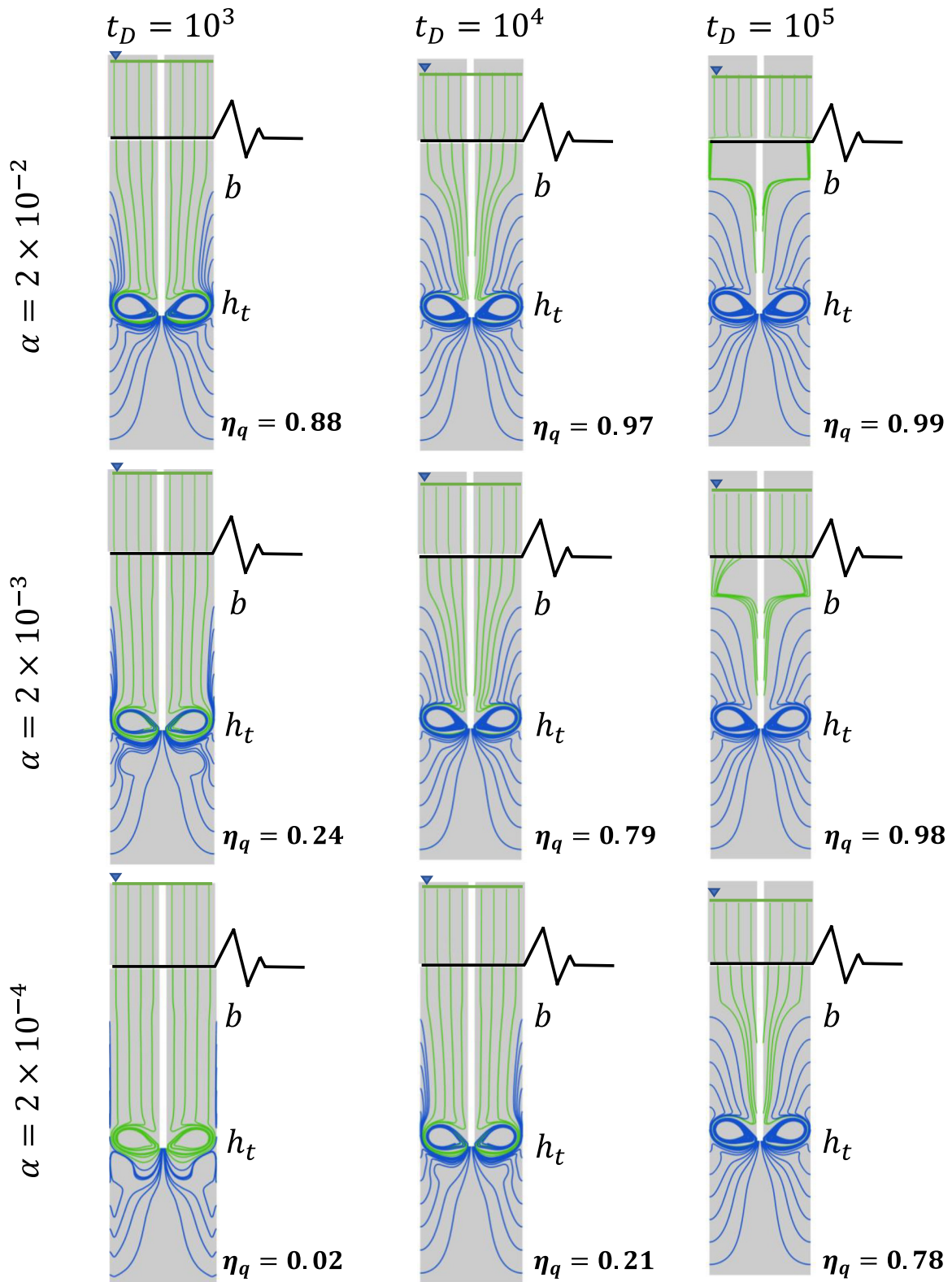### 4.2. Wellbore and Aquifer Drawdown

We compare our numerical model, which incorporates wellbore flow and non-Darcy flow, with two classic Darcy flow solutions to examine wellbore and aquifer drawdown behavior. The first solution is Theis solution, which assumes an infinitely small well radius and considers all pumped water to be from the formation (Theis, 1935), that is, no green streamlines from the casing in Figure 2. Although the Theis solution is widely used, it has limitations at early times and near the wellbore due to these assumptions (Mueller & Witherspoon, 1965). The second solution is the Papadopulos solution, which is more complex but realistic as it takes into account wellbore storage (Papadopulos & Cooper, 1967). Both solutions assume linear flow governed by Darcy's law (DL) in 1-D radial flow models and neglect the mixing process inside the well. Despite these simplifications, they provide valuable insights into the spatial and temporal changes in drawdown behavior. The wellbore drawdown solutions for these two linear flow cases are:

$$S_D = W(r_D, t_D) \tag{14}$$

$$S_D = F(r_D, t_D, \alpha) \tag{15}$$

where Equations 14 and 15 represent the Theis solution and Papadopulos solution, respectively. Notably, the latter includes the dimensionless variable of aquifer storativity α. Aquifers with higher storativity exhibit a more rapid and significant response in formation inflow.

Figure 3 illustrates the behavior of wellbore drawdown at various stages of pumping, comparing the numerical results with the Theis and Papadopulos solutions. In the early stages of pumping, the numerical results of the non-Darcy flow case and the Papadopulos solution show good agreement as they both account for wellbore

Figure 2. Wellbore flow field with different aquifer storativity α at time $t_D = 10^3$, 10^4, and 10^5. Blue streamlines are aquifer inflow and green streamlines are downward casing flow.
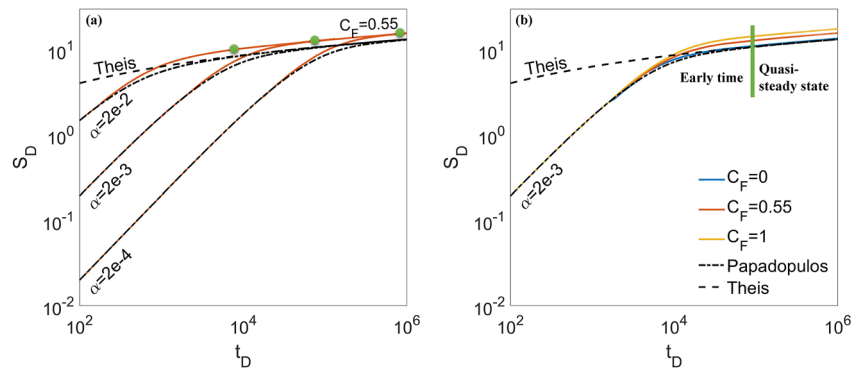
Figure 3. Wellbore drawdown S_D from numerical simulations for nonlinear flow and analytical solutions for linear flow. Green dots and line illustrate the time when reaching quasi-steady state. (a) Cases with different α. (b) Cases with different C_F.

storage, while the Theis solution predicts a much larger drawdown. As pumping continues, the two Darcy flow cases gradually converge and overlap at late times, with the Papadopulos solution approach the Thesis solution, indicating a reduction in well storage effects. In contrast, the non-Darcy flow case gradually deviates from the Darcy flow cases, resulting in a higher drawdown due to the increased pressure head gradient required to overcome the nonlinear term in the flow equation. As the system approaches a quasi-steady state and the wellbore storage effect diminishes, the non-Darcy flow case does not converge to the Darcy cases. These behaviors are consistently observed in Figure 3a for cases with varying aquifer storativity α and Figure 3b for cases with different Forchheimer coefficient C_F.

Figure 3a shows that for a given C_F, the system with a higher α reaches the quasi-steady state more quickly ($t_D \approx 10^4, 10^5$, and 10^6 for $\alpha = 2 \times 10^{-2}, 2 \times 10^{-3}$, and 2×10^{-4}, respectively). However, all cases approach the same asymptotic value of drawdown, indicating that the asymptotic value is not controlled by aquifer storativity. Figure 3b presents different cases with various C_F values, representing different degrees of nonlinearity in the flow. At $C_F = 0$, representing a Darcy flow regime in the aquifer coupled with a RANS wellbore domain, the drawdown simulated by the numerical model closely matches the Papadopulos solution. The slight deviation is due to the wellbore flow, which will be discussed in Section 4.4. As C_F increases from 0 to 1, the deviation of drawdown from the linear case becomes more significant, indicating that the asymptotic drawdown of the quasi-steady state is controlled by the Forchheimer coefficient C_F due to the presence of larger inertial force and drag forces in the porous media, which consume more hydraulic pressure for fluid movement. Despite different C_F values, all cases with $\alpha = 2 \times 10^{-3}$ reach the quasi-steady state at the same time ($t_D \approx 10^5$), further confirming the observation in Figure 3a that α controls the time for the wellbore storage to dissipate and the system to reach the quasi-steady state.

Figure 4 illustrates the aquifer drawdown behavior for different cases with varying values of C_F and α. The temporal behavior of aquifer drawdown follows the same change pattern as the wellbore drawdown shown in Figure 3. In Figure 4a, the aquifer drawdown estimated by Theis solution overestimates the drawdown in the aquifer at $t_D = 10^4$, consistent with the assumption that the aquifer provides 100% water from the start of pumping and well storage is neglected. Figure 4b shows that Theis solution underestimates the drawdown at $t_D = 10^5$ compared to the multiphysics model due to the neglect of flow nonlinearity, which is in line with the behavior shown in Figure 3. Furthermore, larger nonlinearity in the flow leads to deeper cones of depression near the well. At large distances, as evidenced by the subfigure in Figure 4a, the cone with larger C_F ends quicker. This is consistent with the conventional understanding that aquifers of low permeability develop deeper cones of narrower extent. As the distance from the well increases, the drawdown gradually decreases and approaches zero. Figures 4c and 4d shows that nonlinear cases yield larger drawdown compared to the linear cases represented by the Papadopulos solution. This is because the flow surrounding the well encounters more resistance in nonlinear cases. As pumping continues, the drawdown curves for cases with different storativity values converge, indicating the gradual dissipation of the well storage effect and the approach to a late-time solution that is independent of aquifer storativity. At large distances, both the linear and nonlinear cases reach asymptotic results due to the convergence of the ends of the cone of depression. This behavior will be further explained by the variable introduced in Section 4.3.
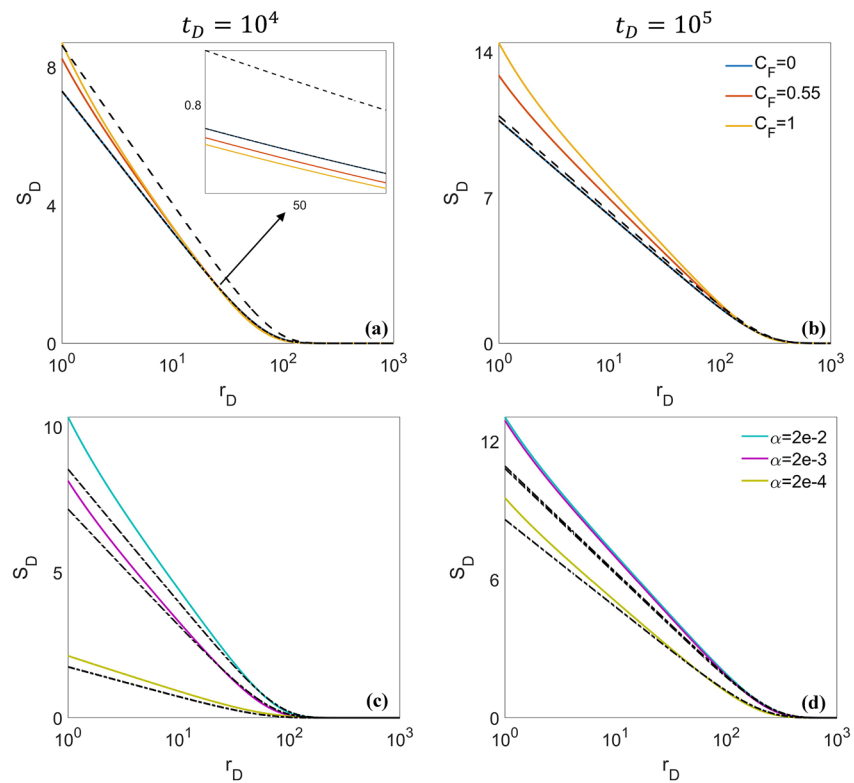
Figure 4. The behavior of aquifer drawdown profiles at different time moments for various cases. (a) $t_D = 10^4$, $\alpha = 2 \times 10^{-3}$, and $C_F = 0$, 0.55, and 1. (b) $t_D = 10^5$, $\alpha = 2 \times 10^{-3}$, and $C_F = 0$, 0.55, and 1. (c) $t_D = 10^4$, $C_F = 0.55$, and $\alpha = 2 \times 10^{-2}$, 2×10^{-3}, and 2×10^{-4}. (d) $t_D = 10^5$, $C_F = 0.55$, and $\alpha = 2 \times 10^{-2}$, 2×10^{-3}, and 2×10^{-4}. Black dashed lines are Theis solution, and black dash-dotted lines are the Papadopulos solution.
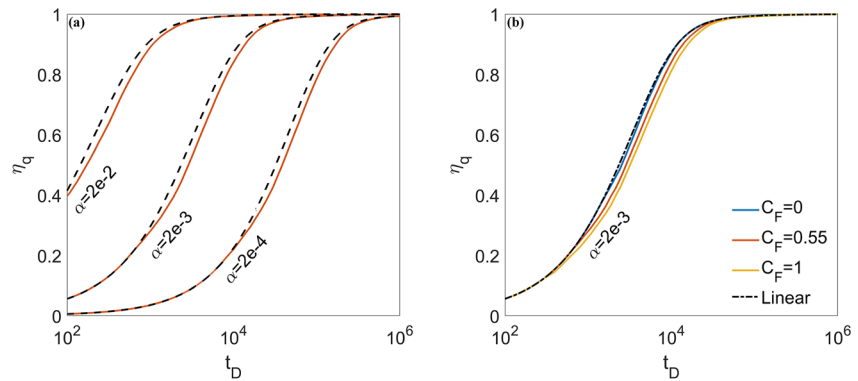
4.3. Water Flow Ratio

To quantify the contributions of different water sources to the pumped water, the water flow ratio is defined as the ratio of aquifer inflow, Q_{aq}, to the total pumping rate, Q (He et al., 2022; Hou & Luo, 2019):

$$\eta_q = \frac{Q_{aq}}{Q} = 1 - \frac{Q_w}{Q} = 1 - \frac{1}{\alpha} \frac{\partial S_{wD}}{\partial t_D} \tag{16}$$

$$Q = Q_{aq} + Q_w \tag{17}$$

where S_{wD} is the normalized wellbore drawdown, and the sum of Q_w and Q_{aq} is the pumping rate Q. The value of η_q ranges from 0 to 1, with higher values indicating a greater contribution from aquifer inflow. It should be noted that η_q for the two linear flow cases can be analytically derived from Equations 14 and 15. However, since Theis solution completely neglects wellbore storage and assumes the abstraction well is a vertical line, η_q is always 1. Therefore, only the Papadopulos solution has a valid water flow ratio curve.

Figure 5a shows the gradual increase of η_q from 0 to 1. The effect of well storage is influenced by aquifer storativity α, with lower α resulting longer response times, consistent with the behavior observed in Figure 2. In particular, the first column of Figure 2 shows that the model with the lowest storativity $\alpha = 2 \times 10^{-4}$ has $\eta_q = 0.02$, while for the highest α case, 88% of pumped water is from the well casing. As indicated by Equation 2, the nonlinear term in the flow equation is positively correlated with the flux. During the initial stages of pumping, when the formation inflow is minimal, there is little difference between nonlinear and linear flow. However, as pumping continues, the nonlinear flow delays the aquifer to achieve higher inflow, leading to smaller values of η_q compared to the linear case. Once η_q reaches 1, which coincides with the time points where drawdown approaches the late time behavior shown in Figure 3a, the formation inflow at the screen matches the pumping rate, and the well storage effect dissipates as the system reaches a quasi-steady state. Figure 5b presents cases with increasing C_F

Figure 5. Water flow ratio η_q with different α, from numerical simulations for nonlinear flow and analytical solutions for linear flow. (a) Cases with different α. (b) Cases with different C_F.

values, where the simulation results with $C_F = 0$ closely align with the analytical solution for linear flow. Higher values of C_F in non-Darcy flow indicate stronger nonlinearity, resulting in a longer aquifer response time and making it more challenging to abstract water from the aquifer and achieve higher wellbore drawdown, as observed in Figure 3b. The inverse relationship between vertical casing water and horizontal aquifer inflow signifies the difficulty in supplying outflow at the intake from both well storage and aquifer storage. This difficulty is most pronounced in scenarios with high C_F and low α values. Hence, in engineering applications, analyzing the early-time wellbore drawdown behavior is crucial for well design and construction. The variable η_q, which quantifies the contributions of different water sources to the pumped water, is essential and should not be neglected.

4.4. Nonlinearity Ratio

To examine the change of aquifer response induced by nonlinearity in non-Darcy flow, we introduce a dimensionless nonlinearity ratio, R. The flow equation for non-Darcy flow from Equation 2 can be formulated as:

$$\nabla S = \boldsymbol{q_1}\left(\frac{1}{K} + \frac{\beta|\boldsymbol{q_1}|}{K}\right) = \boldsymbol{q_1}\left(\frac{1}{K'}\right) \tag{18}$$

where K' is the equivalent conductivity for a non-Darcy flow scenario (Bear, 1988; Zimmerman et al., 2004). The difference between the original conductivity, K, and the equivalent conductivity, K', is:

$$\Delta K = K - K' \tag{19}$$

Due to the vertical flux being less significant in the aquifer, z component is neglected. The difference is normalized by the original conductivity and rearranged with the help from Equations 12 and 13 to obtain the dimensionless variable, R:

$$R(t_D) = 1 - \frac{1}{1 + \beta_D q_{rD}/2} \tag{20}$$

The nonlinearity ratio, R, ranges from 0 to 1, with 0 representing Darcy flow and 1 representing highly nonlinear flow. Essentially, higher R values indicate a decrease in the equivalent conductivity of nonlinear flow, which requires a larger hydraulic gradient for flow movement near the well and leads to larger drawdown, as observed in Figure 3b. It is important to note that R is a time-dependent function due to the transient nature of q_{rD}. At the quasi-steady state during late time, radial aquifer flow dominates the pumped water, and by considering continuity at each cylindrical cross-section, we can approximate q_{rD} as:

$$|q_{1r}| = \frac{Q}{2\pi br} \tag{21}$$

$$q_{rD} = \frac{2}{r_D} \tag{22}$$

Hence, the expression for R at late time is given by:

$$R(t_D \to \infty) = 1 - \frac{1}{1 + \beta_D/r_D} \tag{23}$$

A threshold value of $R = 5\%$ is defined to determine a critical distance, r_D^{crit}, for distinguishing between nonlinear and linear flow regions. Regions with $R < 5\%$ are governed by DL, while regions with $R \geq 5\%$ are considered nonlinear flow regions. By substituting the threshold value of R into Equation 23, we can obtain the critical distance at quasi-steady state:

$$r_D^{\text{crit}}(t_D \to \infty) = 19 \ \beta_D \tag{24}$$

and

$$\begin{cases} r_D > r_D^{\text{crit}}, & \text{Darcy} \\ r_D \leq r_D^{\text{crit}}, & \text{non–Darcy} \end{cases} \tag{25}$$

Equations 24 and 25 provide a simple criterion to delineate Darcy and non-Darcy zones for a pumping well system. For the parameter values in the base case presented in Table 1, r_D^{crit} at quasi-steady state is calculated to be 12.27. This implies that for the base case, DL is applicable for r values greater than 3.68 m.

Figure 6 shows the spatial and temporal behavior of R (also see Figure S1 in Supporting Information S1). R is not constant but varies spatially, with higher values near the well screen and decreasing values as one moves away from the well ($r_D = 1$). This indicates a transition from nonlinear flow to Darcy flow as groundwater moves farther from the well, where R approaches 0. The nonlinear flow region expands as pumping progresses and eventually approaches the quasi-steady state described by Equation 23. The subfigures in the upper section illustrate that the nonlinear flow regions expand as C_F increases with a higher value of R at the same time. The lower section demonstrates that higher α leads to a faster response of the formation to pumping and a more rapid growth of the nonlinear flow region. The model with the highest α almost reaches the quasi-steady state almost at $t_D = 10^3$, while the nonlinear region for case with the lowest α fails to stabilize even at $t_D = 10^5$ (also shown in Figure S2 in Supporting Information S1).

Figure 7 provides insights into the behavior of the critical distance, r_D^{crit}, as a function of time. It confirms that r_D^{crit} increases over time and approaches a steady-state value, as defined by Equation 24. This observation reinforces the understanding that the nonlinear flow region expands as pumping progresses and eventually reaches a quasi-steady state. Additionally, Figure 7 demonstrates that aquifers with higher values of C_F have larger nonlinear regions and yield large values of r_D^{crit} at late times. This suggests that the presence of stronger nonlinearity in the flow, represented by higher C_F values, extends the nonlinear flow region and requires larger critical distances for delineating Darcy and non-Darcy zones. On the other hand, the figure also illustrates that aquifers with higher values of aquifer storativity α, r_D^{crit} approaches the quasi-steady state more quickly due to the faster response time of the aquifer storage to the pumping and a more rapid establishment of the steady-state condition.

### 4.5. Entrance Velocity Profile

Figures 8a–8c shows the velocity profiles along the well screen for models with different C_F values of 0.2, 0.55, and 1. Smaller C_F values lead to larger velocity magnitudes during the initial pumping stage and faster aquifer response times. The numerical model reveals that q_{rD} is not uniformly distributed along the well screen. Instead, the peak value occurs at the height of the pump intake, which is the center of the screen ($z_D = 0.5$). The vortex formed at the intake height (as seen in Figure 2) accelerate the inflow velocity below the intake and decelerate the inflow velocity above the intake. This entrance velocity profile is consistent with field experimental data collected by Church and Granato (1996), Elci et al. (2001), and VonHofe and Helweg (1998). We believe it is a widespread phenomenon, especially for high pumping rates, which correspond to non-Darcy flow in the aquifer and turbulent flow in the wellbore. The disproportionately distributed stress field at the screen passes to the aquifer domain, where 2-D flow occurs in the vicinity of the wellbore. The resistance encountered by groundwater particles is amplified by increasing nonlinearity of the flow, resulting in smaller value of η_q. As pumping
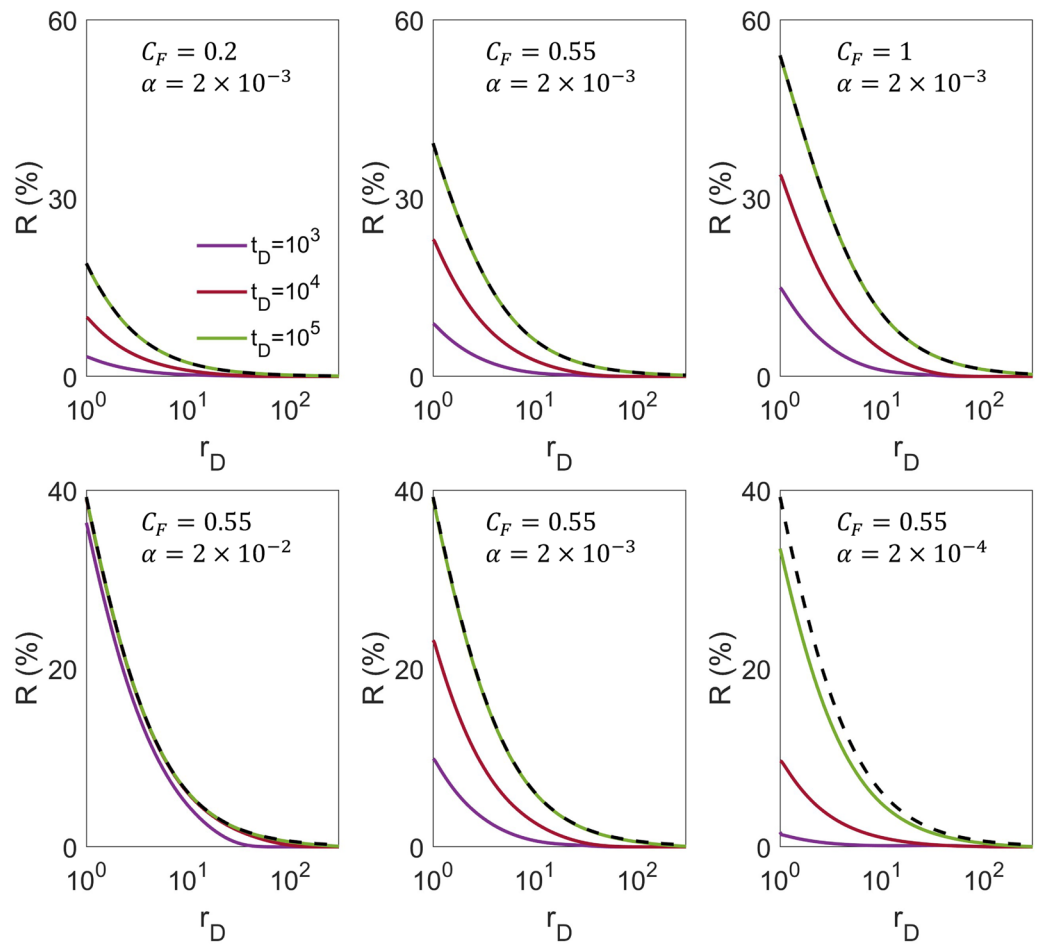
Figure 6. Simulated nonlinear flow regions with various combinations of C_F and α at $t_D = 10^3$, 10^4, and 10^5. Dashed black lines represent R at quasi-steady state.

progresses to late times, q_{rD} approaches 2 for all cases (excluding the intake height where vortex acceleration and deceleration of q_{rD} occur), as illustrated in Equation 22. The pumped out water is 100% of the formation water as a results of η_q reaching 1.

Figures 8d–8f highlights that, given the same nonlinearity of the flow, the varying inflow velocity distribution along the screen creates varying aquifer response time. The model with the highest pumping rate Q produces the largest inflow spike, while the model with a lower pumping rate $0.6Q$ has the smallest spike, resulting in more
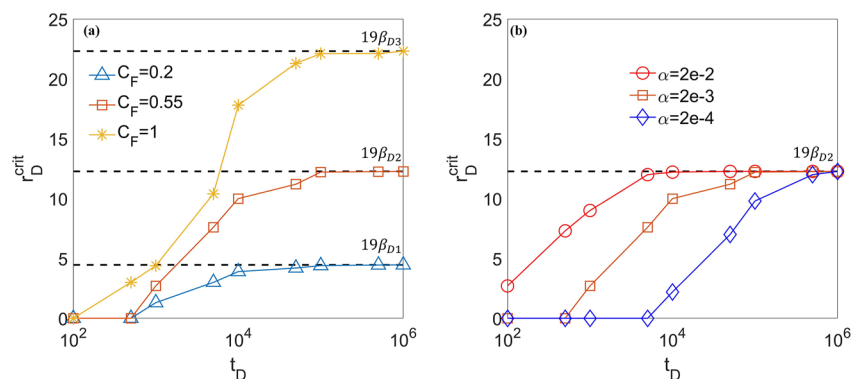
Figure 7. Transient behavior of r_D^{crit} (a) Effect of C_F; and (b) Effect of α.
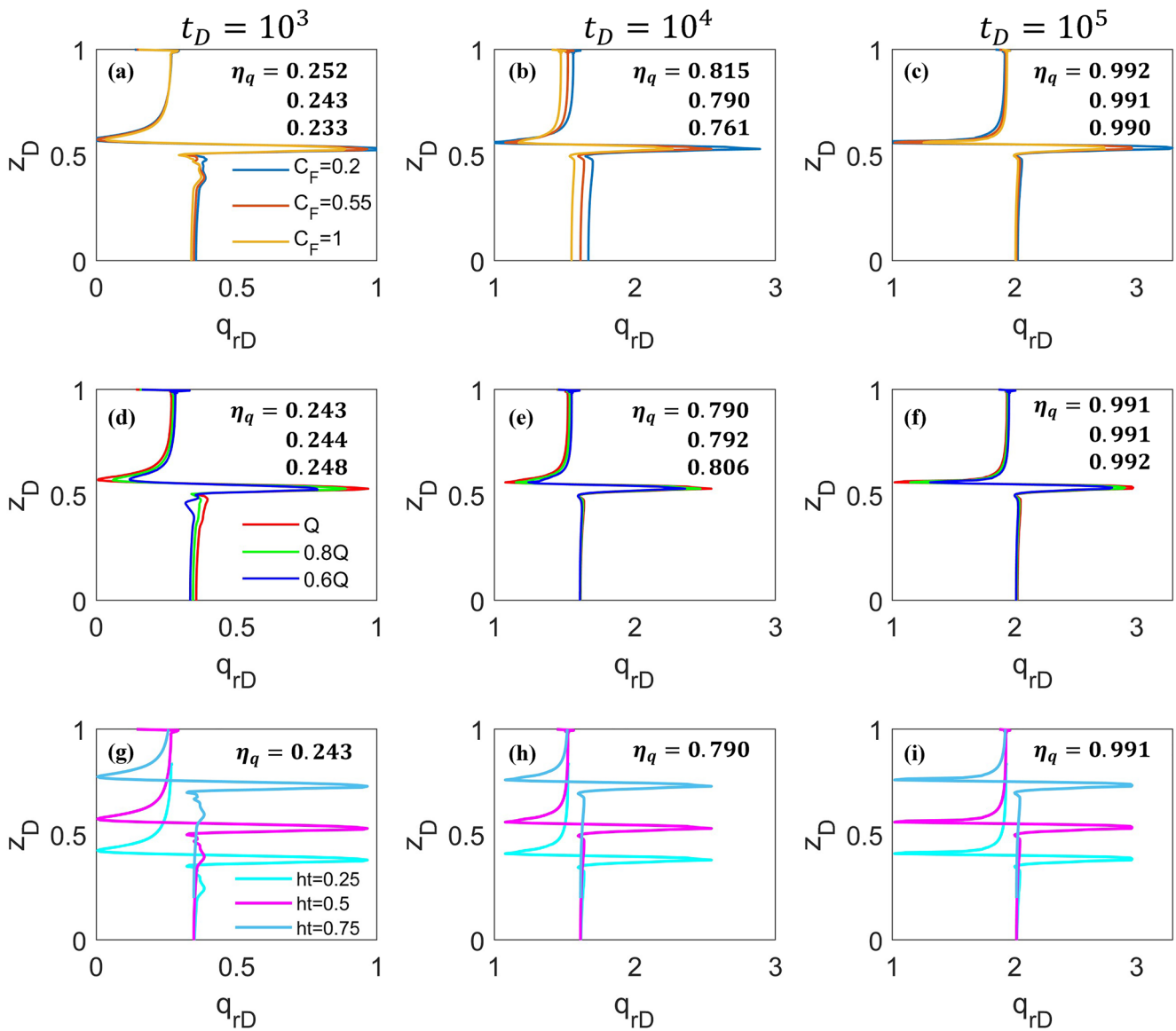
Figure 8. Numerical model inflow velocity profile along the screen. $z_D = z/b$ is the dimensionless height where $z_D = 0$ is at the bottom and $z_D = 1$ is at the top of the screen. The pump intake is placed at the center of the screen, that is, $z_D = 0.5$. Cases with varies C_F, Q and h_t at three time frames are presented.

formation vertical flow being generated and increasing the travel distance for water particles toward the well. To conclude, when there is a smaller inflow spike at the screen, it leads to a quicker aquifer response time (resulting in a larger η_q for smaller Q) and fewer vertical flow in the formation, indicating that wellbore storage is a more tangible source compared to aquifer storage at larger pumping rates. It should be noted that the effect of the larger spike is overshadow by the decreased nonlinearity in cases with different C_F. Simulations with different pump intake positions (h_t) in the screen were conducted. As shown in Figures 8g–8i, the entrance velocity profiles demonstrate a similar trend as previously observed, with a peak value at the intake height and non-uniform distribution along the screen. While the peak value moves with intake position height, the overall hydraulic performance of the well remains the same, as indicated by identical wellbore drawdown S_D and η_q in Figure S4 in Supporting Information S1. This occurs because although velocity profiles change, the nonlinearity of the flow and the spikiness of the inflow velocity remain constant. In other words, the aquifer response time and wellbore drawdown are unaffected by changes in intake position height. However, it is worth noting that the variation of the flow field with intake position could produce different concentration responses if solute transport inside the well were considered.

Pumping in well casing is simulated and presented in Supporting Information S1. Based on the results in Figure S5 in Supporting Information S1, when the intake is positioned above the screen by half of the screen length, there is a slight non-uniformity in the formation inflow. However, the aquifer response time remains unaffected by the intake position. The entrance velocity profile exhibits an increasing trend from the bottom to the top of the screen, with a 2% deviation between the top and the bottom. The field study conducted by VonHofe and Helweg (1998) observed a larger deviation of 40% in the entrance velocity profile between the top and the bottom. It is important to note that the field study positioned the pump intake above the screen by only one-tenth of the screen length in a smaller well. As the intake is moved closer to the screen, the impact of the vortex formation and the irregular distribution of the stress field along the screen become more significant, potentially leading to a more pronounced non-uniformity in the entrance velocity profile and affecting the overall hydraulic behavior within the well system.

5. Simplified Model

5.1. 1-D Flow Model

Previous works investigating wellbore storage effects have mostly neglected the flow and mixing process inside the well and assumed that the inflow velocity is distributed uniformly along the screen. Therefore, conceptual models presented in Figure 1 typically adopt 1-D models with the outlet boundary at the screen defined based on the assumption that the pumping rate is equal to the sum of the rate of formation inflow and the rate of decrease in volume of well storage (e.g., Papadopulos & Cooper, 1967). To facilitate comparison with the 2-D axisymmetric multiphysics model simulation results, we present a simplified 1-D mathematical model that couples non-Darcy flow and well storage effects without accounting for the wellbore flow field.

Assuming that the flux is uniformly distributed along the radial cross section and that the formation water is released from the aquifer as the pressure head declines, the continuity equation Equation 1 in axisymmetric cylindrical coordinates can be expressed as follows:

$$\frac{\partial S_D}{\partial t_D} = -\frac{1}{4r_D}\frac{\partial}{\partial r_D}(r_D q_{rD}) \tag{26}$$

subjected to boundary and initial conditions:

$$\frac{1}{\alpha}\frac{\partial S_{wD}}{\partial t_D} + \frac{1}{2}q_{wD} = 1 \tag{27}$$

$$S_{wD} = S_D(1,t), \qquad q_{wD} = q_{rD}(1,t) \tag{28}$$

$$S_D(r_{eD}, t_D) = 0 \tag{29}$$

$$S_D(r_D, 0) = 0 \tag{30}$$

The flow Equation 2 becomes:

$$\frac{1}{2}\beta_D q_{rD}^2 + q_{rD} + \frac{\partial S_D}{\partial r_D} = 0 \tag{31}$$

where r_{eD} is the radial coordinate of the constant head boundary, q_{rD} [L/T] is the 1-D radial flux.

5.2. 1-D Finite-Difference Approach

The finite-difference method has been widely applied to study non-Darcy flow to an injection/production well (Ewing et al., 1999; Ewing & Lin, 2001; Kolditz, 2001). In order to provide a computationally cheaper alternative to the finite-element model, we propose a 1-D finite-difference approach to directly solve for the behavior of nonlinear flow in a pumping system. The aquifer domain is discretized into J circular cross sections in an axisymmetric cylindrical coordinate system, spaced logarithmically. The first section ($j = 1$) is at the screen and the last section ($j = J$) is at the constant head boundary of a large distance from the well. Odd numbered sections (*i*th) are designated as monitoring wells, where transient drawdowns are analyzed, while the flux at even numbered sections is defined as the continuum representation between two adjacent monitoring wells. The entire system is
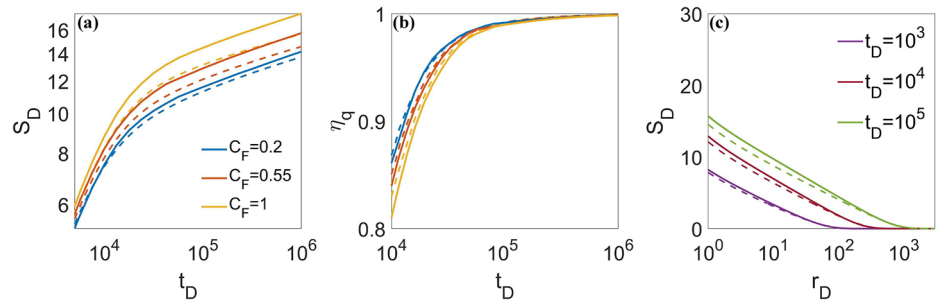
Figure 9. Comparison between 2-D multiphysics numerical model (solid lines) and 1-D finite-difference approach (dashed lines). (a) Wellbore drawdown. (b) Water flow ratio. (c) Aquifer drawdown with $C_F = 0.55$.

then represented mathematically by a set of ordinary differential equations formulated at each section. Notice that all variables subscripted with i and j are dimensionless from Equations 26–31.

$$\frac{\partial S_i}{\partial t_D} \approx -\frac{(r_{2i}q_i - r_{2i-2}q_{i-1})}{4r_{2i-1}(r_{2i} - r_{2i-2})} \quad i = 2, 3, 4 \ldots \frac{J-1}{2} \tag{32}$$

Non-Darcy flux passes through a monitoring well would be:

$$q_i = \frac{1}{\beta_D}\left\{-1 + [1 - 2\beta_D\left(\frac{S_{i+1} - S_i}{r_{2i+1} - r_{2i-1}}\right)]^{\frac{1}{2}}\right\} \quad i = 1, 3, 4 \ldots \frac{J-1}{2} \tag{33}$$

The constant head boundary (r_J) is implemented as:

$$\frac{\partial S_{(J+1)/2}}{\partial t_D} = 0 \tag{34}$$

At the well screen ($r_{wD} = r_1$), from Equation 27, we have:

$$\frac{\partial S_1}{\partial t_D} \approx \alpha\left(1 - \frac{q_1}{2}\right) \tag{35}$$

We compared the finite-difference approach with two published methods (Mathias et al., 2008; Wen et al., 2008) for simulating non-Darcy flow in pumping scenarios, and provided detailed discussion in Text S1 and S2 and Figure S3 in Supporting Information S1.

5.3. Comparison With the 2-D Axisymmetric Numerical Model

While our 1-D finite-difference approach effectively delineates the drawdown behaviors at early times and demonstrates that nonlinearity results in more resistance to flow near the well, it does not account for the effects of wellbore flow field. The presence of wellbore flow field can modify the inflow velocity profile and introduce 2-D flow phenomena in the aquifer, including radial and vertical flow, as discussed in the previous section.

Figure 9a compares the results of 2-D multiphysics simulations and the 1-D finite-difference solution. The numerical model predicts a larger wellbore drawdown, indicating that well storage provides more water at early times. This is further supported by Figure 9b, which shows that the aquifer response time is slower in the finite-difference approach, indicating a smaller value of η_q. Discrepancies in the results approximately begin to appear at $t_D = 10^4$ and stop growing at $t_D = 10^5$, which is the same period when nonlinear flow deviates from Darcy flow (as shown in Figures 2 and 4) because η_q is large enough to amplify effect from the wellbore flow and the aquifer flow nonlinearity. Moreover, larger C_F values result in wider gaps between the two approaches, suggesting that the discrepancy grows with higher levels of nonlinearity. These observations are attributed to the presence of unidentified 2-D flow effects.

Entrance velocity profiles in Figures 8a–8c show that the spikes pass to the aquifer domain and yield 2-D flow. This results in groundwater particles traveling longer paths to the screen and experience larger resistance

compared to the 1-D flow model. To compensate for the slower aquifer response time, more casing water from the well storage must be pumped out during this period, leading to larger wellbore drawdown. The resistance induced by the longer path line is amplified by increasing nonlinearity of the flow, enhancing the discrepancy between the 1-D finite-difference approach and the 2-D numerical model depicted in Figure 9. The gap between the two stops growing as a results of η_q reaching 1 at quasi-steady state, which means that the well storage effect dissipates. Similar trends can be observed in Figure 9c, that is, the 2-D flow effect is amplified as aquifer inflow becomes the predominant source of the pumped water and ends as reaching quasi-steady state. Spatially, the discrepancy diminishes as moving away from the well due to the transition to the 1-D uniform flow at large distances.

6. Conclusions

The present study develops a novel multiphysics numerical model to investigate the hydraulic behavior of well systems considering wellbore storage effects and non-Darcy flow. To quantify wellbore storage effects, the study uses a RANS model coupled with a moving free surface to simulate the turbulent flow and drawdown in the wellbore. Hydraulic behavior investigated include drawdown in the pumping well and aquifer, pumped water ratio, aquifer flow nonlinearity ratio, and wellbore flow field. These hydraulic behaviors are compared with those from simplified 1-D models, including Thesis solution, Papadopulos solution, and a 1-D non-Darcy flow model coupled with well storage effects. The study highlights the following key findings:

- Non-Darcy flow, coupled with the effect of well storage, leads to higher drawdown in the pumping well compared to Darcy flow cases. As the system approaches quasi-steady state, the wellbore drawdown in non-Darcy cases does not converge to Darcy cases. The deviation of the asymptotic drawdown increases with the Forchheimer coefficient C_F. The aquifer drawdown has the same temporal pattern as the wellbore drawdown, but the deviation decreases at large distances due to the limitations of the cone of depression.
- The pumped water ratio, η_q, indicates the challenge of supplying outflow at the intake from aquifer storage. During the initial pumping stage, η_q is almost the same for the multiphysics model and the Papadopulos solution because most of the pumped water comes from well storage. However, as pumping continues, the nonlinear flow has a smaller η_q due to the difficulty of the aquifer to achieve higher inflow compared to the linear case. At late times, η_q reaches 1 as the well storage effect dissipates and the system approaches quasi-steady state. The effect is more significant for large C_F values. Higher aquifer storativity leads to a quicker aquifer response time, causing the wellbore storage effect to dissipate faster, and the system reaches quasi-steady state earlier.
- The nonlinearity ratio, R, measures the disparity between the formation conductivity and the equivalent conductivity of nonlinear flow. A higher value of R indicates increased flow resistance and a smaller equivalent aquifer conductivity. This ratio varies temporally and spatially. As pumping progresses, a quasi-steady state is achieved for the nonlinear flow region, with the transition from non-Darcy flow to Darcy flow occurring further away from the wellbore. By defining a threshold value for R, a critical distance of $19\beta_D$ can be determined to distinguish between the nonlinear and linear flow regions. As the Forchheimer coefficient C_F increases, the nonlinear flow regions expand, indicating a greater influence of non-Darcy flow.
- The presence of a large Reynolds number and turbulent flow around the intake of the pumping well leads to the formation of a vortex in the in-well flow fields. This vortex is observed due to the uneven distribution of stress at the screen, which extends into the aquifer and induces 2-D flow near the well. As a result, groundwater particles travel longer paths to reach the screen, leading to increased hydraulic pressure consumption compared to the 1-D finite-difference approach. This phenomenon is more pronounced at higher pumping rates and larger values of C_F, but diminishes as the wellbore storage is depleted. The height of the intake within the well has a significant impact on the wellbore flow field. Pumping inside the screen promotes more 2-D formation flow, while adjusting the intake position higher in the casing results in a more uniform entrance velocity profile.

The study contributes to our understanding of the hydraulic behavior of well systems in high Reynolds number scenarios by simultaneously considering turbulent flow in the wellbore and non-Darcy flow in the aquifer for the first time, and provides insights for various geophysical engineering activities. In particular, the presence of nonlinearity of the flow and wellbore storage effect increases well and aquifer drawdown, and delays the time for system to reach quasi-steady state. Mueller and Witherspoon (1965) suggested that the Theis solution can be used to predict the pressure response at radius ratios of 20 or above, or after a dimensionless time of 50, but the validity

of its application needs to be re-evaluated in the context of pumping tests or well interference tests involving non-Darcy flow. Based on the study's findings, it is recommended to use the Theis solution at a greater distance away from the well or after a longer pumping time for nonlinear flow conditions. It shall be noticed that the study focuses on high Reynolds number scenarios only. However, by replacing RANS with NS and Non-Darcy with Darcy flow, the coupled multiphysics model is also applicable for accessing concentration response and optimizing groundwater sampling techniques at low Reynolds number. Future research directions include exploring the application of the model to stratified aquifers and heterogeneous fields, as well as investigating concentration responses and optimizing groundwater sampling techniques. The study does not consider well loss and skin effect in the simulation, both of which may have significant effects in practice. Field and laboratory investigations are needed to validate and further explore the hydraulic behavior of pumping well systems in high Reynolds number scenarios.

Data Availability Statement

All data presented in this study were simulated using COMSOL Multiphysics®, a commercial finite element analysis and solver software, https://www.comsol.com. No additional data from external sources were used in the analysis. The comprehensive data set underlying this research article is available for access through the open-access repository, as outlined in He et al. (2023).

References

Bear, J. (1988). *Dynamics of fluids in porous media*. Dover.

Bear, J. (2012). *Hydraulics of groundwater*. Courier Corporation.

Chen, C., Wan, J., & Zhan, H. (2003). Theoretical and experimental studies of coupled seepage-pipe flow to a horizontal well. *Journal of Hydrology*, *281*(1–2), 159–171. https://doi.org/10.1016/S0022-1694(03)00207-5

Chen, Z. X., Lyons, S. L., & Qin, G. (2001). Derivation of the Forchheimer law via homogenization. *Transport in Porous Media*, *44*(2), 325–335. https://doi.org/10.1023/A:1010749114251

Church, P. E., & Granato, G. E. (1996). Bias in ground-water data caused by well-bore flow in long-screen wells. *Groundwater*, *34*(2), 262–273. https://doi.org/10.1111/j.1745-6584.1996.tb01886.x

Elci, A., Molz, F. J., & Waldrop, W. R. (2001). Implications of observed and simulated ambient flow in monitoring wells. *Groundwater*, *39*(6), 853–862. https://doi.org/10.1111/j.1745-6584.2001.tb02473.x

Ewing, R. E., Lazarov, R. D., Lyons, S. L., Papavassiliou, D. V., Pasciak, J., & Qin, G. (1999). Numerical well model for non-Darcy flow through isotropic porous media. *Computational Geosciences*, *3*(3–4), 185–204. https://doi.org/10.1023/A:1011543412675

Ewing, R. E., & Lin, Y. P. (2001). A mathematical analysis for numerical well models for non-Darcy flows. *Applied Numerical Mathematics*, *39*(1), 17–30. https://doi.org/10.1016/S0168-9274(01)00042-3

Forchheimer, P. (1901). Wasserbewegung durch Boden. *Zeitschrift des Vereines Deutscher Ingenieuer*, *45*, 1782–1788.

Gutentag, E. D., Heimes, F. J., Luckey, R. R., & Weeks, J. B. (1984). Geohydrology of the High Plains aquifer in parts of Colorado, Kansas, Nebraska, New Mexico, Oklahoma, South Dakota, Texas, and Wyoming.

Hantush, M. S. (1959). Non-steady flow to flowing wells in leaky aquifers. *Journal of Geophysical Research*, *64*(6), 690. https://doi.org/10.1029/JZ064i008p01043

He, Y., Guo, Q., Liu, Y. Z., Huang, H. Y., Hou, D. Y., & Luo, J. (2023). COMSOL - Pumping well under high Reynolds number flow conditions [Dataset]. Zenodo. https://doi.org/10.5281/zenodo.8217685

He, Y., Hou, D. Y., Huang, H. Y., & Luo, J. (2022). On the ideal groundwater sampling window by utilizing transition pumping period. *Journal of Hydrology*, *610*, 127796. https://doi.org/10.1016/j.jhydrol.2022.127796

Hou, D. Y., & Luo, J. (2019). Proof-of-concept modeling of a new groundwater sampling approach. *Water Resources Research*, *55*(6), 5135–5146. https://doi.org/10.1029/2018wr024227

Huang, H., & Ayoub, J. (2008). Applicability of the Forchheimer equation for non-Darcy flow in porous media. *SPE Journal*, *13*(1), 112–122. https://doi.org/10.2118/102715-Pa

Irmay, S. (1958). On the theoretical derivation of Darcy and Forchheimer formulas. *Eos, Transactions American Geophysical Union*, *39*(4), 702–707. https://doi.org/10.1029/TR039i004p00702

Joseph, D. D., Nield, D. A., & Papanicolaou, G. (1982). Nonlinear equation governing flow in a saturated porous medium. *Water Resources Research*, *18*(4), 1049–1052. https://doi.org/10.1029/WR018i004p01049

Kolditz, O. (2001). Non-linear flow in fractured rock. *International Journal of Numerical Methods for Heat & Fluid Flow*, *11*(5–6), 547–575. https://doi.org/10.1108/EUM0000000005668

Kundu, P. K., Cohen, I. M., & Dowling, D. R. (2015). *Fluid mechanics*. Academic Press.

Launder, B. E., & Spalding, D. B. (1974). The numerical computation of turbulent flows. *Computer Methods in Applied Mechanics and Engineering*, *3*(2), 269–289. https://doi.org/10.1016/0045-7825(74)90029-2

Li, Q., Ito, K., Wu, Z. S., Lowry, C. S., & Loheide, S. P. (2009). COMSOL multiphysics: A novel approach to ground water modeling. *Groundwater*, *47*(4), 480–487. https://doi.org/10.1111/j.1745-6584.2009.00584.x

Martin-Hayden, J. M., Plummer, M., & Britt, S. L. (2014). Controls of wellbore flow regimes on pump effluent composition. *Groundwater*, *52*(1), 96–104. https://doi.org/10.1111/gwat.12036

Mathias, S. A., Butler, A. P., & Zhan, H. B. (2008). Approximate solutions for Forchheimer flow to a well. *Journal of Hydraulic Engineering-ASCE*, *134*(9), 1318–1325. https://doi.org/10.1061/(Asce)0733-9429(2008)134:9(1318)

McMillan, L. A., Rivett, M. O., Tellam, J. H., Dumble, P., & Sharp, H. (2014). Influence of vertical flows in wells on groundwater sampling. *Journal of Contaminant Hydrology*, *169*, 50–61. https://doi.org/10.1016/j.jconhyd.2014.05.005

Moench, A. F., & Prickett, T. A. (1972). Radial flow in an infinite aquifer undergoing conversion from artesian to water table conditions. *Water Resources Research*, *8*(2), 494–499. https://doi.org/10.1029/WR008i002p00494

Moutsopoulos, K. N., & Tsihrintzis, V. A. (2005). Approximate analytical solutions of the Forchheimer equation. *Journal of Hydrology*, *309*(1–4), 93–103. https://doi.org/10.1016/j.jhydrol.2004.11.014

Mueller, T. D., & Witherspoon, P. A. (1965). Pressure interference effects within reservoirs and aquifers. *Journal of Petroleum Technology*, *17*(04), 471–474. https://doi.org/10.2118/1020-PA

Muskat, M. (1937). The flow of fluids through porous media. *Journal of Applied Physics*, *8*(4), 274–282. https://doi.org/10.1063/1.1710292

Neuman, S. P. (1972). Theory of flow in unconfined aquifers considering delayed response of water table. *Water Resources Research*, *8*(4), 1031–1045. https://doi.org/10.1029/WR008i004p01031

Nield, D. A., & Bejan, A. (2006). *Convection in porous media* (Vol. 3). Springer.

Nielsen, D. M. (2005). *Practical handbook of environmental site characterization and ground-water monitoring*. CRC Press.

Papadopulos, I. S., & Cooper, H. H. (1967). Drawdown in a well of large diameter. *Water Resources Research*, *3*(1), 241–244. https://doi.org/10.1029/WR003i001p00241

Rivlin, R. S., & Rideal, E. K. (1948). Large elastic deformations of isotropic materials IV. Further developments of the general theory. *Philosophical Transactions of the Royal Society of London. Series A, Mathematical and Physical Sciences*, *241*(835), 379–397. https://doi.org/10.1098/rsta.1948.0024

Scheidegger, A. E. (1960). Growth of instabilities on displacement fronts in porous media. *The Physics of Fluids*, *3*(1), 94–104. https://doi.org/10.1063/1.1706009

Selvadurai, A. P. S. (2006). Deflections of a rubber membrane. *Journal of the Mechanics and Physics of Solids*, *54*(6), 1093–1119. https://doi.org/10.1016/j.jmps.2006.01.001

Singha, K., & Loheide, S. P. (2011). Linking physical and numerical modelling in hydrogeology using sand tank experiments and COMSOL multiphysics. *International Journal of Science Education*, *33*(4), 547–571. https://doi.org/10.1080/09500693.2010.490570

Takhanov, D. (2011). Forchheimer model for non-Darcy flow in porous media and fractures.

Theis, C. V. (1935). The relation between the lowering of the piezometric surface and the rate and duration of discharge of a well using ground water storage. *Transactions - American Geophysical Union*, *16*(3), 519–524. https://doi.org/10.1029/TR016i002p00519

Thiruvengadam, M., & Kumar, G. N. P. (1997). Validity of Forchheimer equation in radial flow through coarse granular media. *Journal of Engineering Mechanics-ASCE*, *123*(7), 696–705. https://doi.org/10.1061/(Asce)0733-9399(1997)123:7(696)

VonHofe, F., & Helweg, O. J. (1998). Modeling well hydrodynamics. *Journal of Hydraulic Engineering-ASCE*, *124*(12), 1198–1202. https://doi.org/10.1061/(Asce)0733-9429(1998)124:12(1198)

Wang, Q., & Zhan, H. (2017a). Intrawellbore kinematic and frictional losses in a horizontal well in a bounded confined aquifer. *Water Resources Research*, *53*(1), 127–141. https://doi.org/10.1002/2015WR018252

Wang, Q., & Zhan, H. (2017b). The effect of intra-wellbore head losses in a vertical well. *Journal of Hydrology*, *548*, 333–341. https://doi.org/10.1016/j.jhydrol.2017.02.042

Ward, J. C. (1964). Turbulent flow in porous media. *Journal of the Hydraulics Division*, *90*(5), 1–12. https://doi.org/10.1061/JYCEAJ.0001096

Wen, Z., Huang, G. H., & Zhan, H. B. (2008). An analytical solution for non-Darcian flow in a confined aquifer using the power law function. *Advances in Water Resources*, *31*(1), 44–55. https://doi.org/10.1016/j.advwatres.2007.06.002

Whitaker, S. (1996). The Forchheimer equation: A theoretical development. *Transport in Porous Media*, *25*(1), 27–61. https://doi.org/10.1007/Bf00141261

Wu, Y. S. (2002). An approximate analytical solution for non-Darcy flow toward a well in fractured media. *Water Resources Research*, *38*(3), 5-1. https://doi.org/10.1029/2001WR00713

Yeoh, O. H. (1993). Some forms of the strain energy function for rubber. *Rubber Chemistry and Technology*, *66*(5), 754–771. https://doi.org/10.5254/1.3538343

Zanchini, E., Lazzari, S., & Priarone, A. (2012). Long-term performance of large borehole heat exchanger fields with unbalanced seasonal loads and groundwater flow. *Energy*, *38*(1), 66–77. https://doi.org/10.1016/j.energy.2011.12.038

Zimmerman, R. W., Al-Yaarubi, A., Pain, C. C., & Grattoni, C. A. (2004). Non-linear regimes of fluid flow in rock fractures. *International Journal of Rock Mechanics and Mining Sciences*, *41*(3), 384. https://doi.org/10.1016/j.ijrmms.2003.12.045

References From the Supporting Information

Hoog, F. R. D., Knight, J. H., & Stokes, A. N. (1982). An improved method for numerical inversion of Laplace transforms. *SIAM Journal on Scientific and Statistical Computing*, *3*(3), 357–366. https://doi.org/10.1137/0903022

Ikoku, C. U., & Ramey, H. J. (1979). Transient flow of non-Newtonian power-law fluids in porous-media. *Society of Petroleum Engineers Journal*, *19*(3), 164–174. https://doi.org/10.2118/7139-Pa

Izbash, S. (1931). O filtracii v kropnozernstom material (ground water flow in porous media).

Mathias, S. A., & Moutsopoulos, K. N. (2016). Approximate solutions for Forchheimer flow during water injection and water production in an unconfined aquifer. *Journal of Hydrology*, *538*, 13–21. https://doi.org/10.1016/j.jhydrol.2016.03.048

Wen, Z., Liu, K., & Chen, X. L. (2013). Approximate analytical solution for non-Darcian flow toward a partially penetrating well in a confined aquifer. *Journal of Hydrology*, *498*, 124–131. https://doi.org/10.1016/j.jhydrol.2013.06.027